Title

S-Nitrosylation Induces Structural and Dynamical Changes in a Rhodanese Family Protein

Journal

Journal of Molecular Biology, 428(19)

ISSN

0022-2836

Authors

Eichmann, Cédric

Tzitzilonis, Christos

Nakamura, Tomohiro

et al.

Publication Date

2016-09-01

DOI

10.1016/j.jmb.2016.07.010

Peer reviewed

HHS Public Access

Author manuscript

J Mol Biol. Author manuscript; available in PMC 2017 January 24.

Published in final edited form as:

J Mol Biol. 2016 September 25; 428(19): 3737–3751. doi:10.1016/j.jmb.2016.07.010.

S-Nitrosylation Induces Structural and Dynamical Changes in a Rhodanese Family Protein

Cédric Eichmann[1,†], **Christos Tzitzilonis**[2,†], **Tomohiro Nakamura**[3], **Witek Kwiatkowski**[2], **Innokentiy Maslennikov**[2], **Senyon Choe**[2], **Stuart A. Lipton**[3,4,5], and **Roland Riek**[1,2]

[1]Laboratory of Physical Chemistry, Swiss Federal Institute of Technology, ETH-Hönggerberg, CH-8093 Zürich, Switzerland [2]Structural Biology Laboratory, Salk Institute for Biological Studies, La Jolla, CA 92037, USA [3]Neurodegenerative Disease Center, Scintillon Institute, San Diego, CA 92121, USA [4]Department of Neurosciences, University of California, San Diego, School of Medicine, La Jolla, CA 92093, USA [5]Department of Molecular and Experimental Medicine, The Scripps Research Institute, La Jolla, CA 92037, USA

Abstract

S-Nitrosylation is well established as an important post-translational regulator in protein function and signaling. However, relatively little is known about its structural and dynamical consequences. We have investigated the effects of S-nitrosylation on the rhodanese domain of the *Escherichia coli* integral membrane protein YgaP by NMR, X-ray crystallography, and mass spectrometry. The results show that the active cysteine in the rhodanese domain of YgaP is subjected to two competing modifications: S-nitrosylation and S-sulfhydration, which are naturally occurring *in vivo*. It has been observed that in addition to inhibition of the sulfur transfer activity, S-nitrosylation of the active site residue Cys63 causes an increase in slow motion and a displacement of helix 5 due to a weakening of the interaction between the active site and the helix dipole. These findings provide an example of how nitrosative stress can exert action at the atomic level.

Graphical Abstract

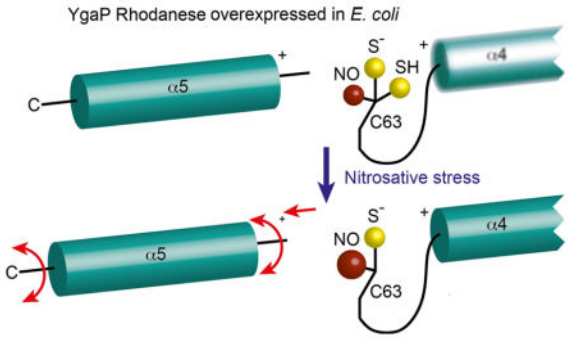

Correspondence to Roland Riek: Laboratory of Physical Chemistry, Swiss Federal Institute of Technology, ETH-Hönggerberg, CH-8093 Zürich, Switzerland. roland.riek@phys.chem.ethz.ch.

†C.E. and C.T. contributed equally to this work.

Keywords

rhodanese; post-translational modification; nuclear magnetic resonance (NMR); X-ray crystallography; mass spectrometry

Introduction

S-nitrosylation has emerged as an important regulator of protein function, comparable to other post-translational modifications such as phosphorylation or acetylation [1–3]. Hence, S-nitrosylation plays an important role in signal transduction pathways [2,4–7] but may also cause disorders, including Alzheimer's and Parkinson's diseases [1,8–12]. In addition, nitric oxide (NO), which is a minor by-product of anaerobic metabolism [13,14], is used by microorganisms as a component of host defense mechanisms [15]. While S-nitrosylation is involved in increasing or inhibiting protein activity, altering protein–protein interactions, affecting protein aggregation, or influencing protein localization [2,4–7], very little is known about its mechanism of action at the atomic level.

S-nitrosylation-induced structure modifications were observed for the first time in crystals of *S*-nitroso-nitrosylhemoglobin [16]. The specific reaction of NO with Cys93β results in a large change of the tertiary structure of the COOH-terminal dipeptide of both β subunits. In addition, X-ray crystallography revealed conformational changes in human thioredoxin-1 [17] and blackfin tuna myoglobin [18]. *S*-nitroso modifications of the cysteines 62 and 69 in *S*-nitrosoglutathione-treated human thioredoxin-1 display planar *cis* geometries, and the accommodation of the SNO groups results in a ~0.5 Å shift of the helix intervening between the two S-nitrosylated cysteines [17]. A reversible conformational helix–loop displacement caused by *in vitro* S-nitrosylation of the surface-exposed Cys10 has been observed in blackfin tuna myoglobin [18]. On the other hand, probing conformational modifications of the stable S-nitrosylated $p21^{Ras}$ GTPase at the solvent-exposed Cys118 by NMR spectroscopy revealed only small chemical shift perturbations of ^{15}N–^{1}H moieties in proximity to Cys118 but no significant secondary or tertiary structural changes [19].

In order to reveal further details in the structural and dynamical changes in proteins upon S-nitrosylation, we selected the rhodanese domain comprising *Escherichia coli* integral membrane protein YgaP for this study. Rhodanese-containing proteins are one of the many protein classes that are targets for S-nitrosylation [20]. Primarily, rhodaneses are involved in the elimination of toxic cyanogenic compounds by catalyzing the transfer of sulfane sulfur from thiosulfate to cyanide, leading to the formation of the less toxic thiocyanate [21,22]. However, it has also been suspected that the ubiquity of the rhodanese domains and their frequent presence in multidomain proteins imply physiological functions other than cell detoxification [21]. The interplay between S-sulfhydration and S-nitrosylation, which are mutually inhibitory processes, is important in H_2S/NO signaling [23]. Therefore, it is interesting that a rhodanese domain can be found in the membrane proteome of *E. coli.* It is located at the cytoplasmic side of the membrane protein YgaP [24] (Fig. 1a). Although the physiological role of YgaP is unknown, the catalytic loop of its rhodanese domain, which includes Cys63, is essential for the sulfur transfer activity [21,22,24]. It has been shown that

S-nitrosylation inactivates the function of rhodanese domains by nitrosylation of the catalytically active Cys [20,23]. Here, we investigated structural and dynamical changes affected by S-nitrosylation *in vitro* by both NMR spectroscopy and X-ray crystallography.

Results

Cys63 of YgaP is the primary S-nitrosylation site

In order to identify whether the membrane protein YgaP from *E. coli* can be S-nitrosylated, we over-expressed, solubilized in detergents, and purified full-length wild-type (WT) YgaP following the protocol described by Tzitzilonis *et al.* [25] and Eichmann *et al.* [24]. The NO-biotin switch assay [26,27] revealed the presence of an S-nitrosylated species of WT YgaP without treatment and the significant increase of S-nitrosylation in the samples treated with a 25-fold molar excess of NO donor *S*-nitrosocysteine (SNOC) for 5 min (Fig. 1b). To elucidate the principal site of S-nitrosylation, we designed two variants YgaP(C158S) and YgaP(C63D,C158S)—denoted here as YgaP^{-} and YgaP^{-}, respectively—to remove the potential nitrosylation site. Both purified variants are correctly folded as determined by NMR [24,25]. While exposure of YgaP^{-} to SNOC (5 mM for 5 min) led to the similar level of S-nitrosylation in treated WT YgaP, no nitrosylation of YgaP^{-} was detected (Fig. 1b). These findings suggest that Cys63 appears to be the primary S-nitrosylation site, which is located in the cytoplasmic rhodanese domain of YgaP (Fig. 1a).

NMR analysis confirms that the rhodanese domain of YgaP is S-nitrosylated *in vivo* and can be further nitrosylated *in vitro* by SNOC treatment

The NO-biotin switch assay also suggests that WT YgaP is partly S-nitrosylated *in vivo* during expression in *E. coli* (Fig. 1b). Therefore, in the 2D [^{15}N,^{1}H]-transverse relaxation optimized spectroscopy (TROSY) [28] NMR spectrum of ^{15}N-labeled rhodanese-F (residues 2–109; Fig. 1a), we expected to find two sets of cross peaks belonging to both the non-modified and the S-nitrosylated protein. Indeed, the minor second set (Fig. 2a) superimposes well with the cross peaks of rhodanese-F treated with 5 mM SNOC (Fig. 2b), which should S-nitrosylate Cys63 according to the NO-biotin switch assay. Sequential assignment allowed the identification of the cross peaks of SNOC-treated rhodanese-F (Fig. 2b). To further verify that Cys63 is the site of S-nitrosylation in the rhodanese domain of YgaP both *in vivo* and *in vitro*, we replaced Cys63 with an Asp. While rhodanese-F(C63D) is still folded [24], the cross peaks attributed to the observed minor, *in vivo* nitrosylated species of rhodanese-F were no longer detected in the 2D [^{15}N,^{1}H]-TROSY spectrum of rhodanese-F(C63D) (Fig. 2c), and as expected, no chemical shift differences between native and SNOC-treated (10 mM) rhodanese-F(C63D) were observed in the 2D [^{15}N,^{1}H]-TROSY spectra (Fig. 2c and d). The absence of slow conformational exchange between the two sets of cross peaks determined by ^{15}N-^{1}H correlated $I_Z S_Z$ chemical exchange experiments [29] and the $^{13}C^{\alpha}$ chemical shift change of Cys63 from 56.9 ppm in native toward 61.6 ppm in SNOC-treated rhodanese-F attributed to the presence of a denser electronic environment for the later species [30] further confirmed the covalent attachment of NO to Cys63 both *in vivo* and *in vitro*.

Mass spectrometry (MS) analysis of rhodanese-F *in vitro* upon SNOC treatment

To further support our findings, we performed MS measurements of ^{15}N-labeled rhodanese-F purified upon overexpression in *E. coli*. In addition to the peak corresponding to the mass of native rhodanese-F (14,200.7; fully ^{15}N-labeled rhodanese-F is 14,205.45), the medium mass electrospray ionization Fourier transform ion cyclotron resonance (ESI FT-ICR) MS analysis shows a peak corresponding to a mass shifted by ~32 Da. This peak is most likely a mixture of two species—the persulfidated protein (+32) and the nitrosylated protein (+30; 15+16−1) (Fig. 3a). However, the resolution of this experiment could not resolve the two. Upon treatment of this sample with 10 mM SNOC for 1 h, which is sufficient to fully nitrosylate the non-modified protein based on the results of the NMR experiment, the non-modified form is indeed absent and its mass is shifted, creating a triply convoluted peak of persulfidated (+32), ^{15}N-labeled S-nitrosylated (+30), and S-nitrosylated (+29) rhodanese-F (Fig. 3b). The question could be raised as to why we did not see a set of separate cross peaks for the persulfidated form in the NMR experiments. The previous study of YgaP S-sulfhydration showed that there is a fast exchange between the S-bound and -unbound states, resulting in a single set of cross peaks [24,31]. In fact, this was the property that made it possible for us to separate S-nitrosylation from S-sulfhydration in the study. Even though the MS analysis could not unambiguously resolve the three species mentioned above, it clearly shows that the SNOC treatment leads to a complete loss of the unmodified protein signal. Thus, in combination with the NO-biotin switch assay and the NMR analysis, this data indicate that the SNOC-treated rhodanese-F is readily S-nitrosylated.

Crystal structures of the rhodanese domain of YgaP reveal that Cys63 is modified by S-nitrosylation and by sulfur

In an attempt to study the 3D structure of the S-nitrosylated form of rhodanese-F, the structure of the untreated crystals obtained from samples prepared with and without 1 mM DTT and the crystals from samples prepared without 1 mM DTT and treated with SNOC were solved to resolutions of 1.62, 1.66, and 1.50 Å (Tables 1 and 2), respectively. The general fold of the native domain (Fig. 4a) is in good agreement with the NMR structure [24]. The r.m.s.d. of the superimposed non-treated X-ray and NMR structures using their respective C^{α} positions is 1.23 Å. The structure of the catalytic loop with the center sulfur of Cys63 together with the C-terminal helix is the hallmark of the rhodaneses. Similar to other rhodanese domains, such as the bovine liver rhodanese [32–35] and GlpE [36], the N–H moieties of the loop are pointing to the sulfur atom of the persulfidated cysteine, which is located above the center of the cradle formed by the backbone of the residues from the catalytic loop (Fig. 4b). In addition to the active site loop, there is an acid–base/hydrophobic surrounding [37,38], with the helix α4 on one side of the catalytic site populated with basic residues (Lys67 and Arg68), the C-terminal helix α5 populated with acidic residues (Glu89 and Asp90), and the bottom of the sandwich guarded by hydrophobic residues (His62 and Leu88; Fig. 4c). Interestingly, the structure of the protein prepared with 1 mM DTT still shows Cys63 modification, which we assigned to S-nitrosylation because this modification is present in both NMR and biotin switch experiments of the native protein (Fig. 5a). The refined geometry of the Cys-NO does not deviate significantly from the ligand restraints, with an S–N bond of 1.60 Å, an S-N-O angle of 118.3°, and a C^{β}-S-N-O dihedral angle of 65.5°. This finding prompts a further question of where NO is coming from and why it is so

stable. The biological role of YgaP is unknown, and it is possible that the protein is designed to stabilize S-NO as part of its function. As expected, the persulfidation is absent in this crystal form. On the other hand, the structure of the protein prepared without DTT shows that the Cys63 has three possible modifications: there is S-NO pointing toward the N terminus of C-terminal helix 5, there is an S-SH modification at the position analogous to other rhodaneses [32,36], and there is a modification pointing toward the N terminus of helix 4, which is most likely another conformation of S-SH (see the argument below; Fig. 5b). When the crystal of the protein from a preparation without DTT was soaked with 1 mM of SNOC for 5 min, the level of S-nitrosylation was slightly higher than in the non-treated X-ray structure (increase from 51% to 64% is based on the respective occupancy factors), the persulfidation level (Cys63-SH) is similar to the one in the non-treated structure, and the modification that was pointing toward the helix 4 disappears. Finally, treating the crystals with thiosulfate resulted in the catalytic cysteine being primarily S-sulfhydrated, and the signal from sulfur pointing toward the N terminus of the α4 helix was significantly enhanced [39]. Therefore, we concluded that this third modification is S-sulfhydration and not S-nitrosylation (Fig. 5c). All three, X-ray, NMR, and MS, show that S-sulfhydration is not SNOC induced.

S-nitrosylation inactivates the enzymatic sulfur transfer activity of the cytoplasmic rhodanese domain of YgaP

The two-step reaction that catalyzes the transfer of sulfane sulfur from thiosulfate ($S_2O_3^{2-}$) to cyanide (CN^-) to form thiocyanate (SCN^-) [24,40] can be monitored by following chemical shift changes of cross peaks near the active site (such as His62, Gln64, Ala65, and Asp90) in the 2D [^{15}N,^{1}H]-TROSY spectra of ^{15}N-labeled rhodanese-F as shown in Eichmann *et al.* [24]. Figure 6 illustrates these findings and shows the chemical shift changes of these residues upon titration with sodium thiosulfate, representing the first step of the enzymatic reaction [24]. It is interesting to note that the minor cross peaks, which have been assigned here to the S-nitrosylated rhodanese-F species, do not shift upon the thiosulfate titration but only change their intensity, indicating competitive replacement by S-sulfhydration. Therefore, the NMR chemical shift analysis demonstrates that S-nitrosylation of Cys63 inactivates the sulfur transfer activity of YgaP.

Structural differences between the native and S-nitrosylated rhodanese domain of YgaP

To investigate the structural consequence of rhodanese-F upon S-nitrosylation, we compared in detail the X-ray structures of untreated and SNOC-treated crystals. The SNOC-treatment reduces the number of alternatives at the catalytic Cys63 from three to two (Fig. 5c). Interestingly, the modification pointing toward helix 4 seems to destabilize the first two turns of that helix, resulting in increased *B*-factors of respective atoms [39]. There are no significant fold differences between the two structures (i.e., the r.m.s.d. of all non-hydrogen atoms between the X-ray structure of non-treated and SNOC-treated is only 0.15 Å). This finding is strengthened by the crystal structure of the C63D variant (at resolution of 1.67 Å), which also has a very similar fold to WT (i.e., the r.m.s.d. of all non-hydrogen atoms between the X-ray structure of WT and C63D is only 0.17 Å), albeit the introduction of a

negatively charged side chain at the active site most likely comes along with a chloride ion at the S^- position.

To further investigate structural alterations induced by S-nitrosylation of rhodanese-F in solution, we measured S-nitrosylation-induced chemical shift changes by solution-state NMR and we mapped these onto the structure of rhodanese-F (Fig. 7a and b). Interestingly, while the detected chemical shift changes were most pronounced for ^{15}N–^{1}H moieties in the active loop (Cys63-Thr69), the adjacent linker (Glu89-Gly91), and the C-terminal helix α5 (Asp93-Lys97), some other regions that are not in close proximity to the catalytic Cys63 (Figs. 2b and 7a and b) also displayed considerable chemical shift changes. In order to decipher the structural alterations induced by S-nitrosylation at atomic resolution, we determined the NMR structure of S-nitrosylated rhodanese-F by following established procedures, including resonance assignment by triple-resonance experiments and the collection of 1936 meaningful nuclear Overhauser enhancement (NOE) distance restraints from 3D ^{13}C- and ^{15}N-resolved [^{1}H,^{1}H]-NOE spectroscopy experiments [41–43]. The set of 20 structures of S-nitrosylated rhodanese-F had a pairwise r.m.s.d. of 0.64 Å for the backbone atoms of residues 2–101 (Fig. 7c and Table 3). There were small residual constraint violations in the final set of the 20 conformers, with the lowest values of the CYANA target function and small deviations from ideal geometry (Table 3). The input data represent a self-consistent set, and the restraints were well satisfied by the calculated conformers. As shown in Fig. 7c, S-nitrosylated rhodanese-F (PDB code **5LAO**) adopts the same fold as the native rhodanese-F [24] comprising a single α/β rhodanese domain [36]. The superposition of the 3D structures of non-treated (blue) and S-nitrosylated (gold) rhodanese-F further highlights that the S-nitrosylation-induced structural changes at the C-terminal helix α5 shifted the helix away from the active site loop. Since nitrosylation reduces the charge in the active site pocket, this structural change is attributed to a weakening of the charge-based interaction between the dipole of the C-terminal helix and the active site.

Dynamical differences between the native and S-nitrosylated rhodanese domain of YgaP

To detect the effect of S-nitrosylation on the dynamics of YgaP, we performed ^{15}N-relaxation measurements and $^{1}H^{N}$ line width analysis on ^{15}N-labeled rhodanese-F with and without SNOC treatment (Fig. 8). Following the procedure by Kay *et al.* [44], similar effective global correlation times of native (7.75 ns) and S-nitrosylated rhodanese-F (7.60 ns) were obtained from relaxation measurements, indicating that both species are monomeric in nature and are well packed. The uniform distribution of the order parameters S^2 for fast motion, with values mostly between 0.8 and 1 and $^{15}N\{^{1}H\}$-NOEs close to 1, implies an overall quite rigid molecular architecture for both species (Fig. 8c), with fast motion only at the N and C termini of rhodanese-F (please note that the relaxation data from native rhodanese-F have been published previously in Ref. [24]). Thus, S-nitrosylation did not have an impact on the fast time-scale motion of rhodanese-F. In contrast, there appeared to be significant differences in dynamics on a slow time scale (μs to ms time range) between native and S-nitrosylated rhodanese-F, as determined from the $^{1}H^{N}$ line width analysis extracted from 2D [^{15}N,^{1}H]-TROSY spectra. In particular, the segments around the active site comprising residues 61–70, as well as the nearby loop (residues 6–10) and the C-

terminal α-helix α5 (residues 90–96), revealed the enhancement of slow conformational dynamics upon S-nitrosylation (Fig. 8a and b). The subset of residues subjected to slow dynamic motion overlaps with that subjected to chemical shift changes (Figs. 7a and 8a). This strong correlation suggests that S-nitrosylation induced the weakening of the charged interaction between the active site and the dipole of the C-terminal helix α5, resulting in a dynamic displacement of the C-terminal helix.

Discussion

The 3D structure of YgaP is composed of a cytoplasmic rhodanese domain and two transmembrane helices forming the interface of a homodimer [24] (Fig. 1a). However, the exact function of this membrane protein still waits to be established. It is known that the active site Cys63 in the 7-aa loop of the rhodanese domain [24] (Fig. 4a) is essential for sulfur transfer catalysis, and similar to other rhodaneses, YgaP transfers the sulfur from thiosulfate to cyanide, leading to the formation of the less toxic thiocyanate [21,22,24]. The crystal structure shows that one of the two conformations of the persulfide group at Cys63 is located above the cradle formed by the active loop sandwiched between two α-helices α4 and α5. The helices are aligned such that their dipoles are stabilizing the persulfide (Fig. 9a). Additionally, the backbone N–Hs of the cradle loop stabilize the persulfide requesting only a limited sequence conservation of the catalytic active loop (Fig. 4b). Therefore, it is quite surprising that the crystal structure reveals an alternative conformation of the persulfide group at Cys63, leading to the destabilization of the N-terminal part of the α5 helix [39] (Fig. 9b). Interestingly, this conformation disappears under nitrosative stress. NMR experiments accompanied with structure determination showed that S-nitrosylation causes small, widespread structural and dynamical alterations. In particular, the change of the charge at the active Cys induced a weakening of the interaction between the active site loop and the dipole of the α5 helix, resulting in a significant structural displacement of this helix (Fig. 9c) accompanied by its increased dynamics. This finding highlights that S-nitrosylation is not only able to inactivate an enzyme through occupying the active site but, by doing so, is also capable of inducing structural and dynamical changes known from other post-translational modifications [45,46]. Overall, the results of this study and our previously published studies [24,39] indicate that there is an intricate interplay between S-nitrosylation and S-sulfhydration, leading to complex structural and dynamic changes, which may play an important role in signaling.

The acid–base/hydrophobic surrounding (Fig. 4c) likely promotes S-nitrosylation by increasing thiol nucleophilicity and concentrating nitrosylating equivalents [3]. However, YgaP lacks an important component of the known C(D,E) S-nitrosylation motif [38]; that is, next to the active Cys, there is a Gln (i.e., Gln64) and not the usual Asp or Glu [38]. Nevertheless, in the X-ray structure, SNO is strongly stabilized by the two N–H backbone hydrogen bonds from Cys63 itself and the conserved Gly66 and by the side chain hydroxyl of Thr69 and solvent molecules. This structural organization is likely to play an essential role in the exceptional stability of S-nitrosylation in YgaP, which is not observed in many other S-nitrosylation reactions [2]. We found that the S-nitrosylated species was present after weeks in the NMR tube, and it survived protein purification upon overexpression in *E. coli.* These remarkable findings not only indicated that S-nitrosylation of YgaP may be

functionally important in *E. coli* but also made it possible to study in great detail the structural and dynamical effects of S-nitrosylation.

Interestingly, the regulation of YgaP is very sensitive to the environment. Our repeated preparations of the protein showed that the initial level of S-nitrosylation varies largely from preparation to preparation and the levels can differ by a factor of 2. While the exact function of YgaP is not yet known, it has been suggested that because of its sulfur transferase activity, YgaP may be involved in transmembrane transport of sulfur and/or sulfur-containing small molecules such as thiocyanate [24]. If so, stress-induced S-nitrosylation would interfere with transmembrane transport, keeping the sulfur content high in the cytoplasm of *E. coli*. This hypothesis is in line with our data suggesting that S-nitrosylation of rhodanese *in vivo* may represent a mechanism whereby NO controls the transfer of sulfane sulfur to various acceptors [24]. Even more importantly, since S-nitrosylation may affect the activity of hundreds or even thousands of different proteins [2], studies of the conformational and dynamical changes induced by this post-translational modification, as revealed here by NMR, may be keys to our understanding of the underlying atomic mechanism of the effects of this redox reaction.

Conclusion

The structural and dynamical investigations of the rhodanese domain of YgaP showed a complex interplay between S-nitrosylation and S-sulfhydration. S-nitrosylation competes with S-sulfhydration and causes inactivation of the enzyme. This process is accompanied by increased dynamics in the regions around the active site. In particular, S-nitrosylation weakens the interaction between helix α5 and the active site, resulting in the displacement of the helix. At the same time, by replacing a persulfide group, S-nitrosylation stabilizes the N-terminal part of the α4 helix destabilized by S-sulfhydration. These findings highlight that S-nitrosylation, like other post-translational modifications [45,46], induces structural and dynamical changes. They also suggest that helix displacement upon nitrosylation may be a prototypical part of a physiological function upon S-nitrosylation in rhodaneses. The present study provides an example of how oxidative/nitrosative stress can cause a change in the structure and dynamics of proteins and suggests that these changes play a widespread and important role in protein action and signaling.

Materials and Methods

Sample preparations

Recombinant WT YgaP, YgaP(C158S), and YgaP(C63D,C158S), which are denoted as $YgaP^{-}$ and $YgaP^{-}$, and the ^{15}N or ^{13}C, ^{15}N-labeled cytoplasmic rhodanese domain of YgaP (called rhodanese-F) and its variant rhodanese(C63D) were overexpressed in the *E. coli* strain BL21 Star™ (DE3) pLysS (Invitrogen, Carlsbad, USA) using standard M9 minimal medium [47] containing 2 g/L ^{13}C Glucose (Isotec) and/or 1 g/L $^{15}NH_4Cl$ (Isotec) in the case of rhodanese-F and rhodanese(C63D). Cells were induced with 0.5 mM IPTG (Invitrogen) at 18 °C and grown for 12 h, and the protein was purified with and without DTT as described previously [25]. The buffer was exchanged to 20 mM Bis-Tris–HCl (pH 7) using a PD10 desalting column. The samples were concentrated with a 10 kDa molecular

weight cut-off Amicon Ultra Centrifugal Filter Device (Milipore) to the final concentration of 1–1.5 mM. For subsequent NMR measurements, 3% D_2O was added.

The samples were S-nitrosylated by the addition of 5 mM SNOC, following a protocol described by Nakamura *et al.* [1].

NO-biotin switch assay

The NO-biotin switch assay was performed as described previously [26,27] with minor modifications. In brief, 3 μg of recombinant YgaP was used for each assay. Blocking buffer {2.5% SDS and 10 mM methyl methane thiosulfonate in HEN buffer [100 mM Hepes (pH 7.4), 1 mM EDTA, and 0.1 mM Neocuproine]} was added to the samples and incubated for 10 min at 50 °C with frequent vortexing to block free thiol groups. After removing excess methyl methane thiosulfonate by acetone precipitation, *S*-nitrosothiols were reduced to thiol with 20 mM ascorbate. The newly formed thiols were linked with the sulfhydryl-specific biotinylating reagent *N*-[6-(biotinamido)hexyl]-3′-(2′-pyridyldithio)propionamide (Thermo Fisher Scientific). For immunoblot analysis, 5 to 10 % of the sample solution was used. Anti-His antibody (Cell Signaling) was used for total YgaP detection, and avidin-HRP (Thermo Fisher Scientific) was used for biotinylated YgaP.

NMR spectroscopy

NMR experiments were performed on a Bruker 700 MHz Avance III spectrometer equipped with a triple-resonance cryoprobe at 30 °C. The spectra were processed with the program PROSA [48] and analyzed with the program XEASY [49]. The sequential assignment and the structure of rhodanese-F were published previously in Eichmann *et al.* [24]. Steady-state heteronuclear $^{15}N–\{^1H\}$-NOE data [44], ^{15}N-relaxation parameters of longitudinal relaxation rates R_1 [50], and transverse relaxation rates $R_{1\rho}$[51] in the rotating frame were measured using standard pulse sequences. R_2 was obtained from R_1 and $R_{1\rho}$. The relaxation measurements were analyzed using the Lipari–Szabo model-free [52] approach implemented in the software package Modelfree 4.15 [53,54]. The analysis yields an effective global correlation time and order parameters S^2 for fast motion.

NMR structure determination

The NMR structure of S-nitrosylated rhodanese-F was determined with the program CYANA [43] (Table 3). A total of 4782 NOE spectroscopy cross peaks were assigned, resulting in 1936 upper distance limits. Backbone torsion angle restraints were obtained from ^{13}C chemical shifts. The standard CYANA protocol of seven iterative cycles of NOE assignment and structure calculation, which was followed by a final structure calculation, was applied [55]. In each cycle, the structure calculation started from 100 randomized conformers, and 10,000 torsion angle dynamics steps were performed per conformer. The 20 conformers with the lowest final CYANA target function values were subjected to restrained energy refinement in explicit solvent using the AMBER force field [56] in the program OPALp [57].

MS analysis

Medium mass ESI-FT-ICR MS analysis was performed on native ^{15}N-labeled rhodanese-F and SNOC-treated, ^{15}N-labeled rhodanese-F (10 mM SNOC for 1 h). Samples were prepared for MS by changing the buffer to 0.1% (vol/vol) acetic acid with a PD-10 desalting column. Calibrated ESI-FT-ICR spectra were collected in positive ion mode on a solariX 94 (Bruker Daltonics) instrument and then deconvoluted to the singly charged species with the Bruker Compass software.

X-ray crystal structure determination

Crystallization trials were conducted with several commercial screening kits, Crystal Screen, Crystal Screen 2 (Hampton Research, CA, USA), Wizard Screens I and II (Emerald BioStructures, WA, USA), PEG/Ion, and Nextal Classics suite (Qiagen, Inc., CA, USA), using the Mosquito crystallization robot (TTP Labtech, MA, USA). The trials yielded several crystallization hits, which were subsequently optimized. The final crystal was obtained using the hanging-drop vapor-diffusion method, in which 1 μl of 10 mg/ml protein was mixed with 1 μl of a reservoir solution of 0.2 M sodium acetate in 0.1 M Tris–HCl (pH 8.5) and 30% polyethylene glycol 4k. Crystals appeared after a few days at 15 °C and were frozen in liquid N_2. To induce S-nitrosylation, we soaked crystals in 1 mM SNOC for 5 min before freezing. For structure solution, we measured data from crystals of protein prepared without DTT and soaked with 0.5 M of NaI in well solution for 1 min [58] and with 100 mM of Gd-HPDO3A (Natx-ray, France) in well solution for 30 s [59]. Diffraction data were collected in-house using a Micromax-007HF X-ray generator (Rigaku, USA). Data were processed with autoPROC/XDS [60]. Phase calculation was completed using the autoSHARP [61] software in the CCP4 program suite 6.1.13 [62]. The iodine and gadolinium atom sites were located with the program SHELXD [63], solvent flattening was performed with SOLOMON [64], and a final model was built with Arp/warp [65]. The statistics of data processing and phasing are listed in Table 1. The coordinates and structure factors of rhodanese-F have been deposited in the PDB with accession codes of 5HBL. The X-ray data of the crystals of rhodanese-F prepared without DTT, the SNOC-treated rhodanese-F, and the C63D variant of rhodanese-F were collected at SSRL on beamline 12–2 and processed by HKL2000 [66]. Model building was done in COOT version 0.8.1 [67]. Refinement of the structures was completed using REFMAC, version 5.8.0124 [68]. The structure figures were generated using Molscript version 2.1.2 [69] and MOLMOL [70]. Coordinates and structure factors for rhodanese-F prepared without DTT, the SNOC-treated rhodanese-F, and the C63D variant of rhodanese-F have been deposited in the PDB with accession codes of 5HBO, 5HBP, and 5HBQ, respectively. The data processing and refinement statistics are in Table 2.

Accession numbers

Coordinates and structure factors have been deposited in the Protein Data Bank with accession numbers: 5HBL, 5HBO, 5HBP, 5HBQ, 5LAM, and 5LAO.

Acknowledgments

This work was supported in part by NIH grants R21 NS080799, P01 HD29587, and R01 NS086890 and by a Distinguished Investigator Award from the Brain & Behavior Research Foundation to S.A.L. The funders had no role in study design, data collection and analysis, decision to publish, or preparation of the manuscript.

Author contributions: C.E. and C.T. prepared protein samples; C.E. and W.K. performed mass spectrometry analysis; C.T. crystallized protein samples; C.T. and W.K. collected and analyzed X-ray data; T.N. performed NO-biotin switch assays; C.E., C.T., and R.R. collected and analyzed NMR data; and C.E., C.T., T.N., W.K., I.M., S.C., S.A.L., and R.R. helped design the experiments, contributed to scientific discussions, and prepared the manuscript.

Conflict of interest: The authors declare that they have no conflicts of interest with the contents of this article.

Abbreviations used

NO	nitric oxide
WT	wild-type
SNOC	*S*-nitrosocysteine
TROSY	transverse relaxation optimized spectroscopy
MS	mass spectrometry
NOE	nuclear Overhauser enhancement

References

1. Nakamura T, Wang L, Wong CCL, Scott FL, Eckelman BP, Han X, Tzitzilonis C, Meng F, Gu Z, Holland EA, Clemente AT, Okamoto S, Salvesen GS, Riek R, Yates JR, Lipton SA. Transnitrosylation of XIAP regulates caspase-dependent neuronal cell death. Mol Cell. 2010; 39:184–195. [PubMed: 20670888]
2. Nakamura T, Tu S, Akhtar MW, Sunico CR, Okamoto SI, Lipton SA. Aberrant protein s-nitrosylation in neurodegenerative diseases. Neuron. 2013; 78:596–614. [PubMed: 23719160]
3. Seth D, Stamler JS. The SNO-proteome: causation and classifications. Curr Opin Chem Biol. 2011; 15:129–136. [PubMed: 21087893]
4. Choi YB, Tenneti L, Le DA, Ortiz J, Bai G, Chen HS, Lipton SA. Molecular basis of NMDA receptor-coupled ion channel modulation by S-nitrosylation. Nat Neurosci. 2000; 3:15–21. [PubMed: 10607390]
5. Qu J, Nakamura T, Cao G, Holland EA, McKercher SR, Lipton SA. S-nitrosylation activates Cdk5 and contributes to synaptic spine loss induced by beta-amyloid peptide. Proc Natl Acad Sci U S A. 2011; 108:14,330–14,335.
6. Shi ZQ, Sunico CR, McKercher SR, Cui J, Feng GS, Nakamura T, Lipton SA. S-nitrosylated SHP-2 contributes to NMDA receptor-mediated excitotoxicity in acute ischemic stroke. Proc Natl Acad Sci U S A. 2013; 110:3137–3142. [PubMed: 23382182]
7. Uehara T, Nakamura T, Yao D, Shi ZQ, Gu Z, Ma Y, Masliah E, Nomura Y, Lipton SA. S-nitrosylated protein-disulphide isomerase links protein misfolding to neurodegeneration. Nature. 2006; 441:513–517. [PubMed: 16724068]
8. Dawson VL, Dawson TM, London ED, Bredt DS, Snyder SH. Nitric oxide mediates glutamate neurotoxicity in primary cortical cultures. Proc Natl Acad Sci U S A. 1991; 88:6368–6371. [PubMed: 1648740]
9. Lipton SA, Choi YB, Pan ZH, Lei SZ, Chen HS, Sucher NJ, Loscalzo J, Singel DJ, Stamler JS. A redox-based mechanism for the neuroprotective and neurodestructive effects of nitric oxide and related nitroso-compounds. Nature. 1993; 364:626–632. [PubMed: 8394509]

10. Huang Z, Huang PL, Panahian N, Dalkara T, Fishman MC, Moskowitz MA. Effects of cerebral ischemia in mice deficient in neuronal nitric oxide synthase. Science. 1994; 265:1883–1885. [PubMed: 7522345]
11. Leist M, Volbracht C, Kühnle S, Fava E, Ferrando-May E, Nicotera P. Caspase-mediated apoptosis in neuronal excitotoxicity triggered by nitric oxide. Mol Med Camb Mass. 1997; 3:750–764. [PubMed: 9407551]
12. Gu Z, Kaul M, Yan B, Kridel SJ, Cui J, Strongin A, Smith JW, Liddington RC, Lipton SA. S-nitrosylation of matrix metalloproteinases: signaling pathway to neuronal cell death. Science. 2002; 297:1186–1190. [PubMed: 12183632]
13. Ji XB, Hollocher TC. Mechanism for nitrosation of 2,3-diaminonaphthalene by *Escherichia coli*: enzymatic production of NO followed by O2-dependent chemical nitrosation. Appl Environ Microbiol. 1988; 54:1791–1794. [PubMed: 3046492]
14. Seth D, Hausladen A, Wang YJ, Stamler JS. Endogenous protein S-nitrosylation in *E. coli*: regulation by OxyR. Science. 2012; 336:470–473. [PubMed: 22539721]
15. MacMicking J, Xie QW, Nathan C. Nitric oxide and macrophage function. Annu Rev Immunol. 1997; 15:323–350. [PubMed: 9143691]
16. Chan NL, Rogers PH, Arnone A. Crystal structure of the S-nitroso form of liganded human hemoglobin. Biochemistry (Mosc). 1998; 37:16,459–16,464.
17. Weichsel A, Brailey JL, Montfort WR. Buried *S*-nitrosocysteine revealed in crystal structures of human thioredoxin. Biochemistry (Mosc). 2007; 46:1219–1227.
18. Schreiter ER, Rodríguez MM, Weichsel A, Montfort WR, Bonaventura J. S-nitrosylation-induced conformational change in blackfin tuna myoglobin. J Biol Chem. 2007; 282:19,773–19,780.
19. Williams JG, Pappu K, Campbell SL. Structural and biochemical studies of p21Ras S-nitrosylation and nitric oxide-mediated guanine nucleotide exchange. Proc Natl Acad Sci U S A. 2003; 100:6376–6381. [PubMed: 12740440]
20. Foster MW, Forrester MT, Stamler JS. A protein microarray-based analysis of S-nitrosylation. Proc Natl Acad Sci U S A. 2009; 106:18,948–18,953. [PubMed: 19106304]
21. Papenbrock J, Guretzki S, Henne M. Latest news about the sulfurtransferase protein family of higher plants. Amino Acids. 2010; 41:43–57. [PubMed: 20135153]
22. Cipollone R, Ascenzi P, Tomao P, Imperi F, Visca P. Enzymatic detoxification of cyanide: clues from *Pseudomonas aeruginosa* rhodanese. J Mol Microbiol Biotechnol. 2008; 15:199–211. [PubMed: 18685272]
23. Kwiecień I, Sokołowska M, Luchter-Wasylewska E, Włodek L. Inhibition of the catalytic activity of rhodanese by S-nitrosylation using nitric oxide donors. Int J Biochem Cell Biol. 2003; 35:1645–1657. [PubMed: 12962704]
24. Eichmann C, Tzitzilonis C, Bordignon E, Maslennikov I, Choe S, Riek R. Solution NMR structure and functional analysis of the integral membrane protein YgaP from *Escherichia coli*. J Biol Chem. 2014; 289:23,482–23,503.
25. Tzitzilonis C, Eichmann C, Maslennikov I, Choe S, Riek R. Detergent/nanodisc screening for high-resolution NMR studies of an integral membrane protein containing a cytoplasmic domain. PloS One. 2013; 8:1–8.
26. Jaffrey SR, Erdjument-Bromage H, Ferris CD, Tempst P, Snyder SH. Protein S-nitrosylation: a physiological signal for neuronal nitric oxide. Nat Cell Biol. 2001; 3:193–197. [PubMed: 11175752]
27. Yao D, Gu Z, Nakamura T, Shi ZQ, Ma Y, Gaston B, Palmer LA, Rockenstein EM, Zhang Z, Masliah E, Uehara T, Lipton SA. Nitrosative stress linked to sporadic Parkinson's disease: S-nitrosylation of parkin regulates its E3 ubiquitin ligase activity. Proc Natl Acad Sci U S A. 2004; 101:10,810–10,814.
28. Pervushin K, Riek R, Wider G, Wüthrich K. Attenuated T2 relaxation by mutual cancellation of dipole–dipole coupling and chemical shift anisotropy indicates an avenue to NMR structures of very large biological macromolecules in solution. Proc Natl Acad Sci U S A. 1997; 94:12,366–12,371.
29. Montelione GT, Wagner G. 2D chemical exchange NMR spectroscopy by proton-detected heteronuclear correlation. J Am Chem Soc. 1989; 111:3096–3098.

30. Schwarzinger S, Kroon GJ, Foss TR, Wright PE, Dyson HJ. Random coil chemical shifts in acidic 8 M urea: implementation of random coil shift data in NMRView. J Biomol NMR. 2000; 18:43–48. [PubMed: 11061227]
31. Wang W, Zhou P, He Y, Yu L, Xiong Y, Tian C, Wu F. Fast conformational exchange beween the sulfur-free and persulfide-bound rhodanese domain of *E. coli* YgaP. Biochem Biophys Res Commun. 2014; 452:817–821. [PubMed: 25204500]
32. Ploegman JH, Drent G, Kalk KH, Hol WG. Structure of bovine liver rhodanese. I. Structure determination at 2.5 A resolution and a comparison of the conformation and sequence of its two domains. J Mol Biol. 1978; 123:557–594. [PubMed: 691057]
33. Ploegman JH, Drent G, Kalk KH, Hol WG. The structure of bovine liver rhodanese. II. The active site in the sulfur-substituted and the sulfur-free enzyme. J Mol Biol. 1979; 127:149–162. [PubMed: 430559]
34. Ploegman JH, Drent G, Kalk KH, Hol WGJ, Heinrikson RL, Keim P, Weng L, Russell J. The covalent and tertiary structure of bovine liver rhodanese. Nature. 1978; 273:124–129. [PubMed: 643076]
35. Trevino RJ, Gliubich F, Berni R, Cianci M, Chirgwin JM, Zanotti G, Horowitz PM. NH2-terminal sequence truncation decreases the stability of bovine rhodanese, minimally perturbs its crystal structure, and enhances interaction with GroEL under native conditions. J Biol Chem. 1999; 274:13,938–13,947.
36. Spallarossa A, Donahue JL, Larson TJ, Bolognesi M, Bordo D. *Escherichia coli* GlpE is a prototype sulfurtransferase for the single-domain rhodanese homology superfamily. Structure. 2001; 9:1117–1125. [PubMed: 11709175]
37. Marino SM, Gladyshev VN. Structural analysis of cysteine S-nitrosylation: a modified acid-based motif and the emerging role of trans-nitrosylation. J Mol Biol. 2010; 395:844–859. [PubMed: 19854201]
38. Stamler JS, Toone EJ, Lipton SA, Sucher NJ. (S)NO signals: translocation, regulation, and a consensus motif. Neuron. 1997; 18:691–696. [PubMed: 9182795]
39. Eichmann, C., Tzitzilonis, C., Kwiatkowski, W., Riek, R. S-sulfhydration of the catalytic cysteine in the rhodanese domain of YgaP is complex dynamic process. Matters. 2016. http://dx.doi.org/10.19185/matters.201602000004
40. Schlesinger P, Westley J. An expanded mechanism for rhodanese catalysis. J Biol Chem. 1974; 249:780–788. [PubMed: 4855815]
41. Wüthrich, K. NMR of Proteins and Nucleic Acids. John Willey & Sons; New York, Chichester, Brisbane, Toronto, Singapore: 1986.
42. Cavanagh, J., Fairbrother, WJ., Palmer, AG., III, Skelton, NJ., Rance, M. Protein NMR Spectroscopy: Principles and Practice. Elsevier Academic Press; 2010.
43. Güntert P, Mumenthaler C, Wüthrich K. Torsion angle dynamics for NMR structure calculation with the new program DYANA. J Mol Biol. 1997; 273:283–298. [PubMed: 9367762]
44. Kay LE, Torchia DA, Bax A. Backbone dynamics of proteins as studied by 15 N inverse detected heteronuclear NMR spectroscopy: application to staphylococcal nuclease. Biochemistry (Mosc). 1989; 28:8972–8979.
45. Xin F, Radivojac P. Post-translational modifications induce significant yet not extreme changes to protein structure. Bioinforma Oxf Engl. 2012; 28:2905–2913.
46. Nussinov R, Tsai CJ, Xin F, Radivojac P. Allosteric post-translational modification codes. Trends Biochem Sci. 2012; 37:447–455. [PubMed: 22884395]
47. Sambrook, J., Fritsch, EF., Maniatis, T. Molecular Cloning: A Laboratory Manual. Cold Spring Harbor Laboratory; Cold Spring Harbor, NY: 1989.
48. Güntert P, Dötsch V, Wider G, Wüthrich K. Processing of multi-dimensional NMR data with the new software PROSA. J Biomol NMR. 1992; 2:619–629.
49. Bartels C, Xia TH, Billeter M, Güntert P, Wüthrich K. The program XEASY for computer-supported NMR spectral analysis of biological macromolecules. J Biomol NMR. 1995; 6:1–10. [PubMed: 22911575]

50. Farrow NA, Muhandiram R, Singer AU, Pascal SM, Kay CM, Gish G, Shoelson SE, Pawson T, Forman-Kay JD, Kay LE. Backbone dynamics of a free and phosphopeptide-complexed Src homology 2 domain studied by 15 N NMR relaxation. Biochemistry (Mosc). 1994; 33:5984–6003.
51. Peng JW, Thanabal V, Wagner G. 2D heteronuclear NMR measurements of spin-lattice relaxation times in the rotating frame of X nuclei in heteronuclear HX spin systems. J Magn Reson. 1991; 1969(94):82–100.
52. Lipari G, Szabo A. Model-free approach to the interpretation of nuclear magnetic resonance relaxation in macromolecules. 1. Theory and range of validity. J Am Chem Soc. 1982; 104:4546–4559.
53. Mandel AM, Akke M, Palmer AG. Backbone dynamics of *Escherichia coli* ribonuclease HI: correlations with structure and function in an active enzyme. J Mol Biol. 1995; 246:144–163. [PubMed: 7531772]
54. Palmer AG III, Rance M, Wright PE. Intramolecular motions of a zinc finger DNA-binding domain from Xfin characterized by proton-detected natural abundance carbon-13 heteronuclear NMR spectroscopy. J Am Chem Soc. 1991; 113:4371–4380.
55. Güntert P, Buchner L. Combined automated NOE assignment and structure calculation with CYANA. J Biomol NMR. 2015; 62:453–471. [PubMed: 25801209]
56. Cornell WD, Cieplak P, Bayly CI, Gould IR, Merz KM, Ferguson DM, Spellmeyer DC, Fox T, Caldwell JW, Kollman PA. A second generation force field for the simulation of proteins, nucleic acids, and organic molecules. J Am Chem Soc. 1995; 117:5179–5197.
57. Koradi R, Billeter M, Güntert P. Point-centered domain decomposition for parallel molecular dynamics simulation. Comput Phys Commun. 2000; 124:139–147.
58. Dauter Z, Dauter M, Rajashankar KR. Novel approach to phasing proteins: derivatization by short cryo-soaking with halides. Acta Crystallogr D Biol Crystallogr. 2000; 56:232–237. [PubMed: 10666615]
59. Girard E, Stelter M, Vicat J, Kahn R. A new class of lanthanide complexes to obtain high-phasing-power heavy-atom derivatives for macromolecular crystallography. Acta Crystallogr D Biol Crystallogr. 2003; 59:1914–1922. [PubMed: 14573945]
60. Vonrhein C, Flensburg C, Keller P, Sharff A, Smart O, Paciorek W, Womack T, Bricogne G. Data processing and analysis with the autoPROC toolbox. Acta Crystallogr D Biol Crystallogr. 2011; 67:293–302. [PubMed: 21460447]
61. Vonrhein C, Blanc E, Roversi P, Bricogne G. Automated structure solution with autoSHARP. Methods Mol Biol (Clifton NJ). 2007; 364:215–230.
62. Winn MD, Ballard CC, Cowtan KD, Dodson EJ, Emsley P, Evans PR, Keegan RM, Krissinel EB, Leslie AGW, McCoy A, McNicholas SJ, Murshudov GN, Pannu NS, Potterton EA, Powell HR, Read RJ, Vagin A, Wilson KS. Overview of the CCP4 suite and current developments. Acta Crystallogr D Biol Crystallogr. 2011; 67:235–242. [PubMed: 21460441]
63. Sheldrick GM. A short history of SHELX. Acta Crystallogr A. 2008; 64:112–122. [PubMed: 18156677]
64. Abrahams JP, Leslie AGW. Methods used in the structure determination of bovine mitochondrial F1 ATPase. Acta Crystallogr D Biol Crystallogr. 1996; 52:30–42. [PubMed: 15299723]
65. Perrakis A, Morris R, Lamzin VS. Automated protein model building combined with iterative structure refinement. Nat Struct Mol Biol. 1999; 6:458–463.
66. Otwinowski, Z., Minor, W. Processing of X-ray Diffraction Data Collected in Oscillation Mode”Methods in Enzymology. In: Carter, CW., Jr, Sweet, RM., editors. Macromolecular Crystallography, part A. Vol. 276. Academic Press; New York: 1997. p. 307-326.
67. Emsley P, Lohkamp B, Scott WG, Cowtan K. Features and development of Coot. Acta Crystallogr D Biol Crystallogr. 2010; 66:486–501. [PubMed: 20383002]
68. Murshudov GN, Skubák P, Lebedev AA, Pannu NS, Steiner RA, Nicholls RA, Winn MD, Long F, Vagin AA. REFMAC5 for the refinement of macromolecular crystal structures. Acta Crystallogr D Biol Crystallogr. 2011; 67:355–367. [PubMed: 21460454]
69. Kraulis PJ. MOLSCRIPT: a program to produce both detailed and schematic plots of protein structures. J Appl Crystallogr. 1991; 24:946–950.

70. Koradi R, Billeter M, Wüthrich K. MOLMOL: a program for display and analysis of macromolecular structures. J Mol Graph. 1996; 14(51–55):29–32.

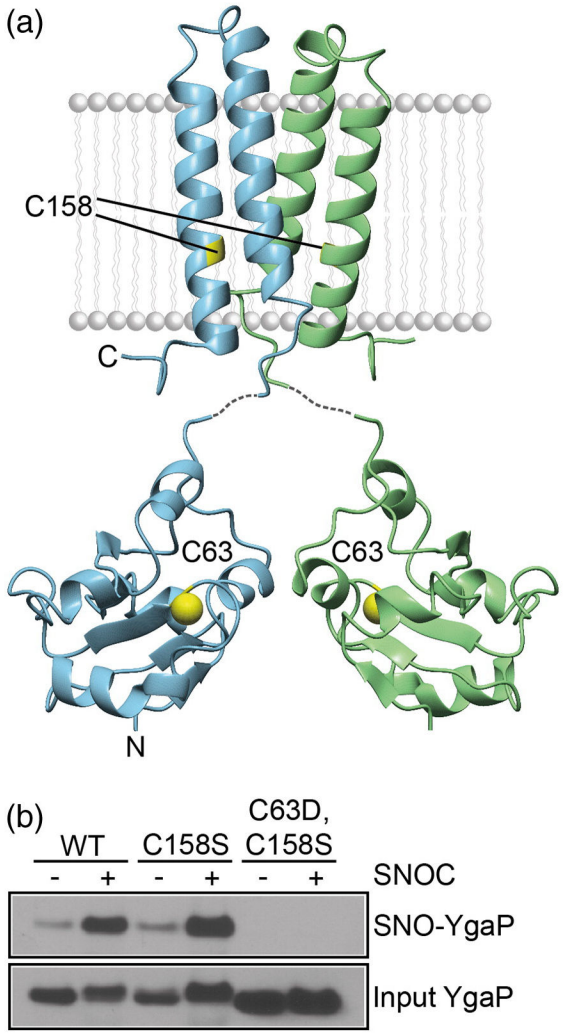

Fig. 1.

Identification of the S-nitrosylation site of YgaP *in vitro*. (a) NMR structure model of full-length YgaP(C158S) embedded in a lipid bilayer [24]. The individual subunits of dimeric YgaP (PDB codes **2MOI** and **2MPN**) are shown individually as blue and green color-coded ribbons. The cysteine residues Cys63 and Cys158 are colored in yellow and labeled. The lipid bilayer is indicated in gray. (b) S-nitrosylation of purified WT YgaP and its variants YgaP(C158S) and YgaP(C63D,C158S), which are denoted in the text as $YgaP^{-}$ and $YgaP^{-}$, is detected by NO-biotin switch assay. S-nitrosylation of the various variants was measured before (−) and upon treatment with SNOC (+). The bottom line shows the Western Blot bands of the proteins indicating the protein amount used.

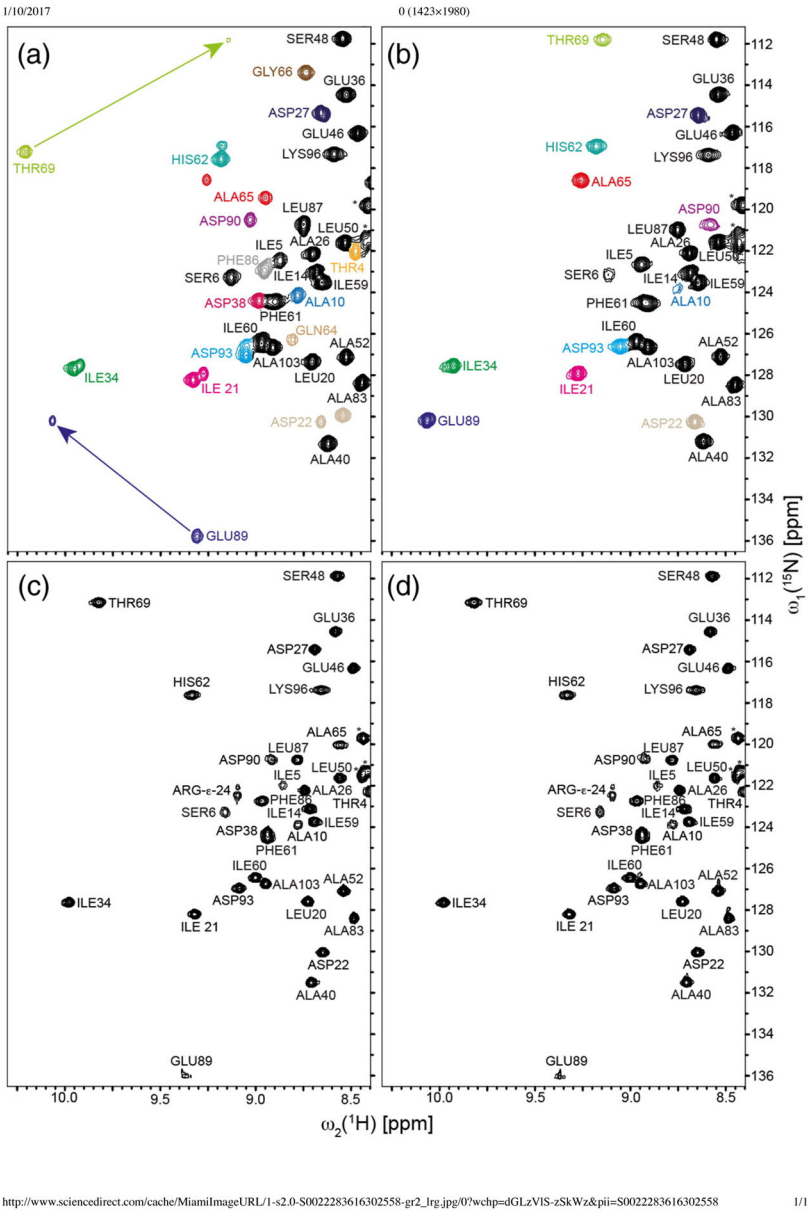

Fig. 2.

NMR analysis of the non-treated and S-nitrosylated rhodanese domain of YgaP. Selection of 2D [^{15}N,^{1}H]-TROSY spectra of (a) non-treated rhodanese-F and its variant (c) rhodanese-F(C63D) and their corresponding (b, d)5 mM SNOC-treated samples. Cross peaks displaying composite chemical shift changes caused by SNOC treatment are colored for individual residues, and the cross peaks of the main species are labeled according to the sequential assignment with the three-letter amino acid code. Cross peaks without chemical shift perturbations are displayed in black and accordingly labeled. Cross peaks identified with * correspond to amino acid residues from the His tag. For the color-coded cross peaks in (a), there exist major and minor species. The cross peaks of the minor species become fully populated in (b) at the cost of the cross peaks of the major species. In contrast, the

minor species is absent in rhodanese-F(C63D) (c), and SNOC treatment of this sample had no effect on the 2D [^{15}N,^{1}H]-TROSY spectrum (d).

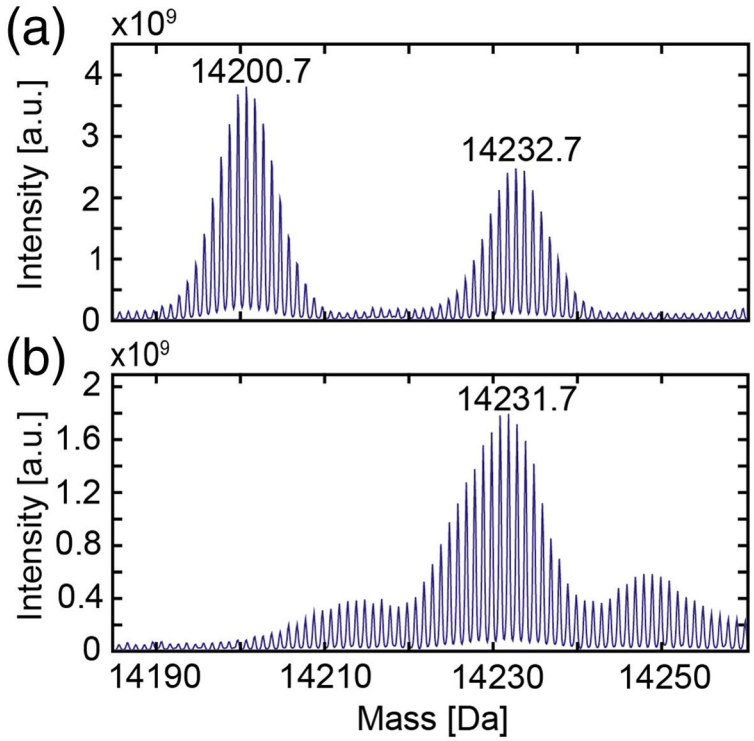

Fig. 3.

MS analysis of rhodanese-F *in vitro* upon SNOC treatment. Deconvoluted mass spectra from ESI FT-ICR MS of (a) non-treated and (b) 10 mM SNOC-treated, ^{15}N-labeled cytoplasmic rhodanese domain.

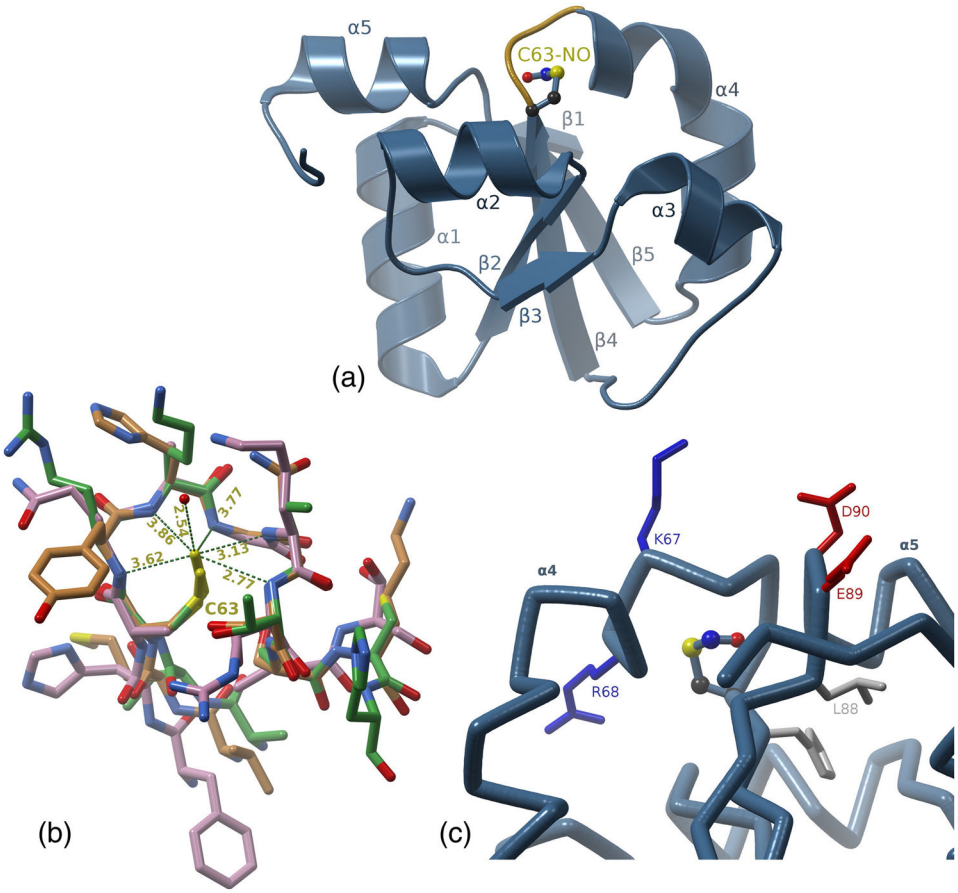

Fig. 4.

X-ray structure analysis of the rhodanese domain of YgaP. (a) General fold of the YgaP rhodanese domain of non-treated crystal showing S-nitrosylation of Cys63. (b) Overlay of the catalytic loop of bovine liver rhodanese (carbon atoms painted green), SNOC-treated crystal of the rhodanese domain of YgaP (carbon atoms painted pink) and GlpE (carbon atoms painted brown). The distances between the Cys63-S^{γ}atom and the backbone amides of the residues from the catalytic loop are given in Å. (c) The acid–base/hydrophobic environment of the S-nitrosylation site in the non-treated rhodanese domain of YgaP.

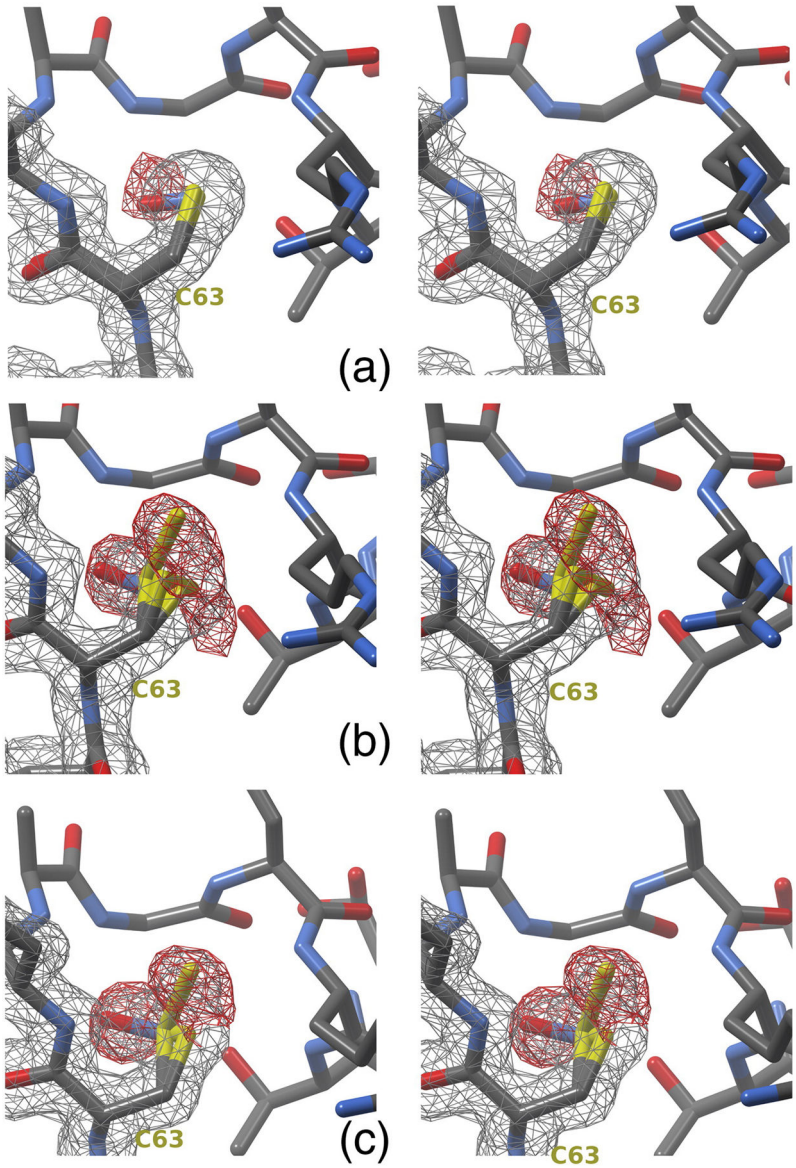

Fig. 5.

The Cys63 modifications observed in X-ray structures. (a) The electron density represented by 2Fo-Fc map (gray at 1σ level) and unbiased Fo-Fc map (red at 3σ level) of the non-treated crystal of the protein prepared with DTT is interpreted as the partial modification of Cys63 with NO. (b) The electron density represented by 2Fo-Fc map (gray at 1σ level) and unbiased Fo-Fc map (red at 3σ level) of the non-treated crystal of the protein prepared without DTT is interpreted as the partial modification of Cys63 with NO and with SH in two different conformations. (c) The electron density represented by 2Fo-Fc map (gray at 1σ level) and unbiased Fo-Fc map (red at 3σ level) of the SNOC-treated crystal of the protein prepared without DTT shows the disappearance of one conformation of SH and the strengthening of the NO modification.

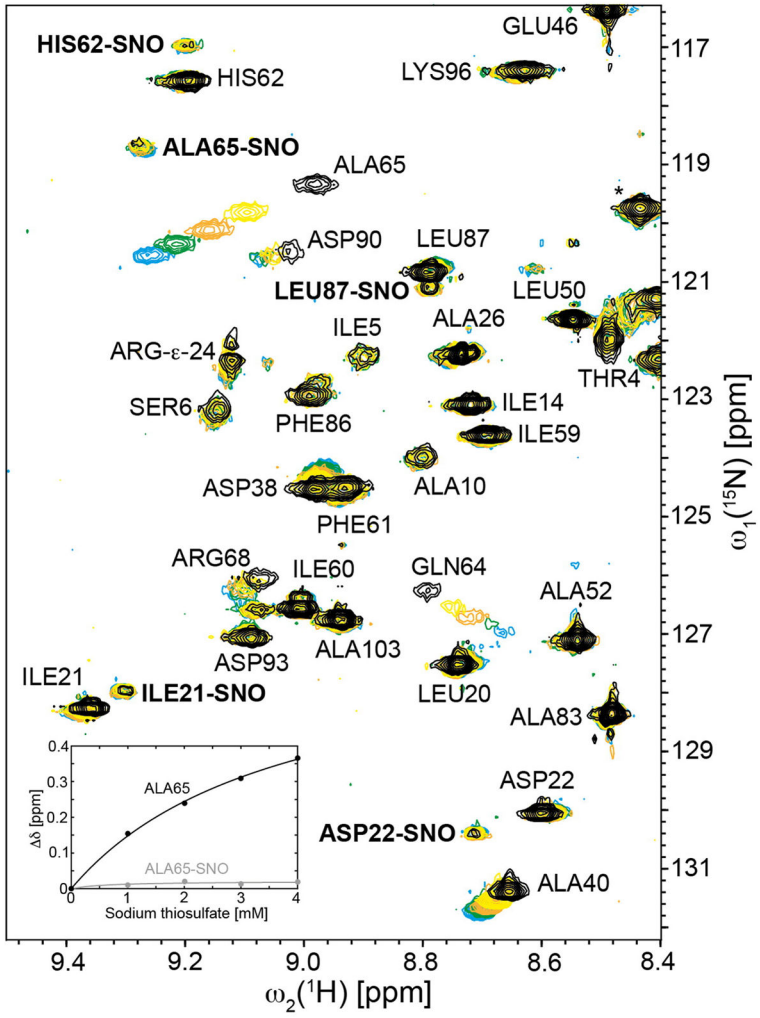

Fig. 6.

Inhibition of the catalytic sulfur transfer activity of S-nitrosylated rhodanese-F. Selection of 2D [^{15}N,^{1}H]-TROSY spectra of rhodanese-F in the absence of sodium thiosulfate (black) and in the presence of 1 mM (yellow), 2 mM (orange), 3 mM (green), and 4 mM (blue) sodium thiosulfate [24]. Chemical shift changes of residues Gln64, Ala65, and Asp90 are indicative of the catalytic sulfur transfer activity of rhodanese-F. There is a set of cross peaks in the spectra labeled with SNO coming from a minor species, which has been identified as the *in vivo* S-nitrosylated rhodanese-F. No chemical shift changes of the cross peaks of this species upon treatment with sodium thiosulfate are observed, indicating that S-nitrosylation inactivates the catalytic activity of rhodanese-F (inset). The cross peak identified with * corresponds to an amino acid residue from the His tag.

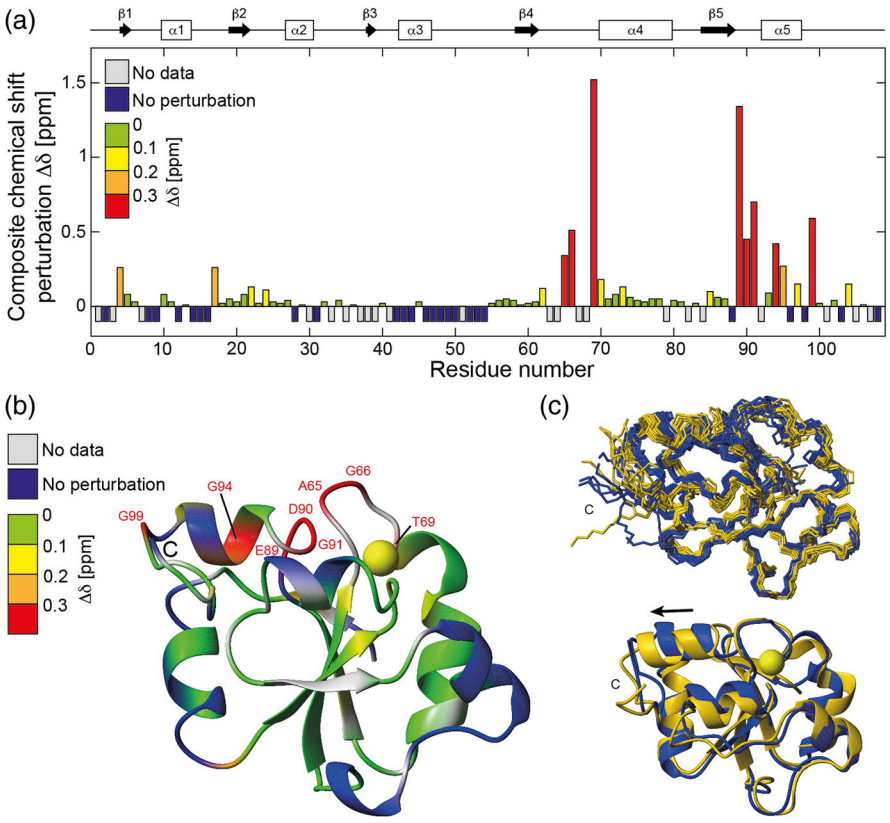

Fig. 7.

Structural changes of the rhodanese domain caused by S-nitrosylation. (a) Composite chemical shift perturbation $\Delta\delta = \sqrt{\Delta\delta_H^2 + (\Delta\delta_N/5)^2}$ of ^{15}N–^{1}H moieties of rhodanese-F induced by S-nitrosylation *versus* the amino acid sequence. A gray or blue bar corresponds to a residue for which no data were obtained or no chemical shift changes were detected, respectively. The secondary structure elements that resulted from NMR analysis [24] are depicted above the graph. (b) The chemical shift perturbations of (a) are mapped onto the refined mean 3D structure of rhodanese-F (PDB code **5LAM**) with the color code indicated in the figure. (c) Polypeptide backbone superposition of the NMR structures of native (blue; PDB code **5LAM**) and S-nitrosylated rhodanese-F (gold; PDB code **5LAO**) is represented by the corresponding bundles of the 10 conformers with the lowest CYANA target function and the ribbon drawings of native (blue) and S-nitrosylated rhodanese-F (gold).

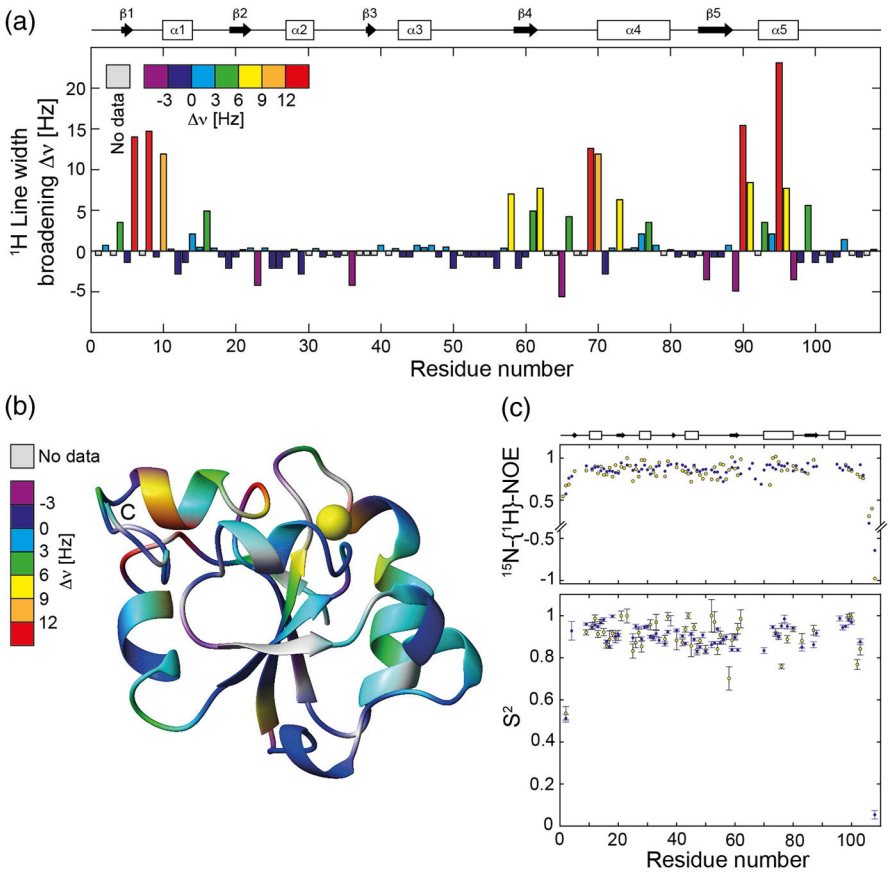

Fig. 8.

Dynamical changes of the rhodanese domain caused by S-nitrosylation. (a) $^{1}H^{N}$ line width comparison between S-nitrosylated and native rhodanese-F along the amino acid sequence, and (b) it is mapped onto the refined mean 3D structure of rhodanese-F (PDB code **5LAM**). The line width change is indicative of a change of slow dynamics. The position of the SH modification is in line with the dipole created by C-terminal helix α5. (c) Residue-resolved, steady-state $^{15}N–\{^{1}H\}$-NOEs and fast order parameters S^2 derived for native [24] (blue) and S-nitrosylated (gold) rhodanese-F. The secondary structure elements as determined by NMR [24] are depicted above the graphs, with α-helices and β-strands shown as open rectangles and filled arrows, respectively.

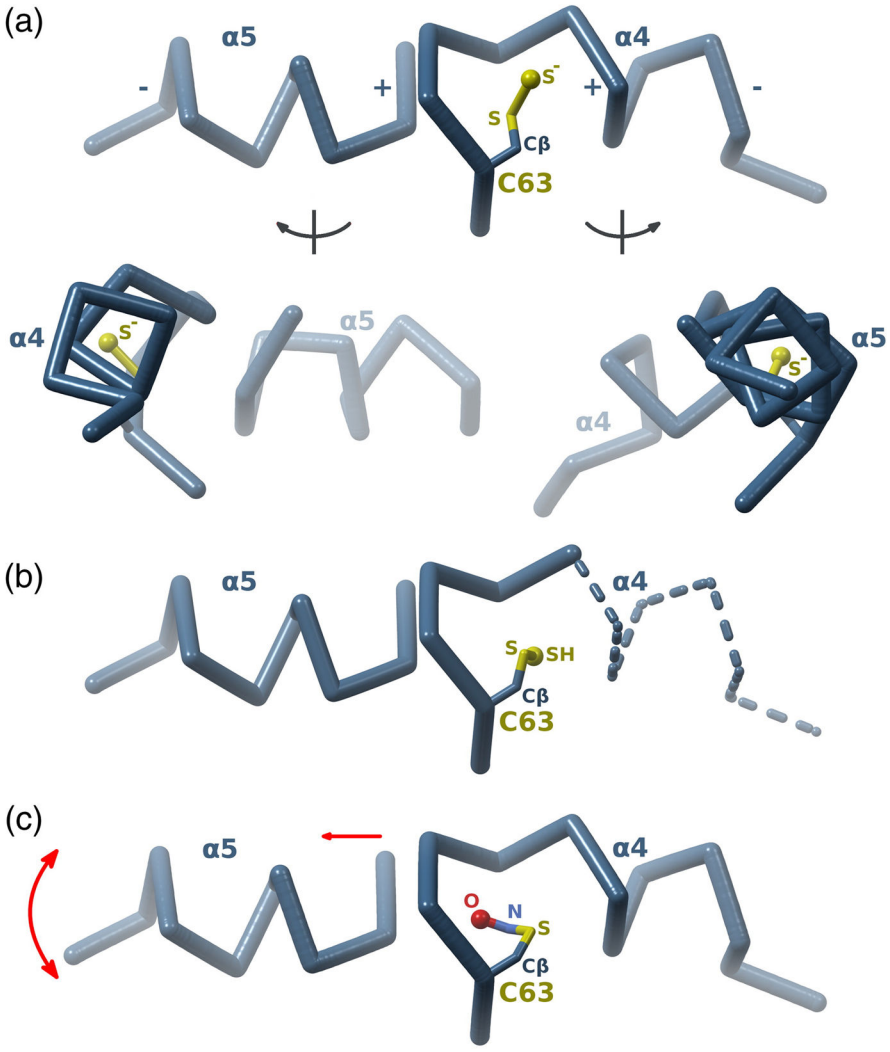

Fig. 9.

Summary of Cys63 modification in YgaP. (a) The persulfide group along and through the helices views show that the two helical dipoles from the α4 and α5 helices are perfectly aligned with the sulfur atom from the persulfide group. (b) The persulfide group in an alternative conformation is destabilizing the α4 helix as indicated by a dashed line. (c) The NO group causes shifting and increased dynamics of the α5 helix as indicated by red arrows.

Table 1

X-ray data processing and phasing statistics

	Native	Gadolinium	Iodine
Data collection (autoPROC)			
Space group	P3 (1)	P3 (1)	P3 (1)
Unit-cell parameters			
a (Å)	43.96	43.99	43.64
c (Å)	52.33	52.81	52.31
Resolution range (Å)	52.3–1.62 (1.62–1.61)	52.8–2.32 (2.45–2.32)	52.3–2.41 (2.42–2.41)
No. of observed reflections	72,412	55,813	47,596
No. of unique reflections	14,075	4912	4212
Signal-to-noise ratio I/σ(I)	34.4(5.9)	27.2(8.9)	25.9(11.5)
Redundancy	5.1(3.1)	11.4(11.3)	11.3(10.7)
Completeness (%)	97.4(70.0)	99.8(99.5)	97.9(91.4)
R_{merge} (%)	0.030(0.180)	0.074(0.293)	0.084(0.188)
Rano (%)	0.027(0.166)	0.042(0.097)	0.077(0.175)
Phasing statistics (autoSHARP)			
No. of sites		2	3
Site occupancies		0.45,0.17	0.57,0.22,0.12
Figure of Merit (FOM) after ML refinement	0.155		
R_{cullis} for acentric reflections		ISO:0.448 ANO:0.860	ISO:0.635 ANO:0.851
Phasing power for acentric reflections		ISO:1.216 ANO:0.865	ISO:0.753 ANO:0.862
FOM after DM [(correlation on E^2)/contrast]	1.8869		
Free *R*-factor in real space	0.266		

Table 2

X-ray data processing and refinement statistics

	Non-treated, prepared with DTT	Non-treated, prepared without DTT	SNOC-treated	C63D
DATA PROCESSING				
Space group	P3 (1)	P3 (1)	P3 (1)	P3 (1)
Unit-cell parameters				
a (Å)	43.96	43.68	43.87	43.90
c (Å)	52.33	52.42	52.64	52.67
Resolution range (Å)	52.3–1.62 (1.62–1.61)	37.8–1.66 (1.75–1.66)	38.0–1.50 (1.53–1.50)	38.0–1.66 (1.75–1.66)
No. of observed reflections	72,412	70,404	82,067	69,348
No. of unique reflections	14,075	13,034	16,889	13,404
$<I>/\sigma(I)$	34.4(5.9)	28.1(6.6)	18.7(1.9)	15.3(2.0)
Redundancy	5.1(3.1)	5.4(4.2)	4.9(2.4)	5.2(4.0)
Completeness (%)	97.4(70.0)	98.6(91.3)	93.9(61.5)	99.6(98.0)
R_{merge}	0.030(0.180)	0.037(0.197)	0.082(0.490)	0.068(0.670)
REFINEMENT				
No. of atoms	985	1006	997	926
No. of solvent atoms	149	143	147	98
No. of residues	105	103	103	103
R	0.20	0.18	0.17	0.19
R_{free}	0.24	0.20	0.18	0.22
r.m.s. bonds	0.009	0.007	0.009	0.012
r.m.s. angles	1.36	1.32	1.50	1.58
Average *B*-factor (Å2)	18.60	18.64	17.41	19.58
main chain	15.26	15.96	14.35	17.61
side chain	17.79	17.71	16.74	19.87
solvent	30.44	29.57	28.18	26.70
Ramachandran favored (%)	91.2	93.3	93.3	92.1
Ramachandran allowed (%)	8.8	6.7	6.7	7.9
Ramachandran outliers (%)	0	0	0	0

Table 3

Experimental NMR data and structural statistics

Quantity				Rhodanese-F	SNO-Rhodanese-F
Restraints	H-bonds			0	0
	NOE distances	intra-residue		500	560
		sequential		477	441
		medium range		355	339
		long range		528	596
	Dihedral angles			100	94
Residual distance restraint violations					
	Number >0.2 Å			0	0
	Maximum			0.12 ± 0.11 Å	0.11 ± 0.01 Å
Residual dihedral angle restraint violations					
	Number >5°			0	0
	Maximum			3.7 ° ± 1.0 °	0.8 ° ± 0.9 °
Residual dihedral angle restraint violations				0	0
Backbone r.m.s.d.	Residues		2–101	0.59 Å	0.64 Å
Heavy atom r.m.s.d.	Residues		2–101	1.01 Å	1.14 Å
Ramachandran plot	Residues in most favored regions			71%	77%
	Residues in additionally allowed regions			24%	21%
	Residues in generously allowed regions			3%	2%
	Residues in disallowed regions			2%	0%